Producing H_2-Rich Gas from Simulated Biogas and Applying the Gas to a 50W PEFC Stack

Guangwen Xu, Xin Chen, Kazunori Honda, and Zhan-Guo Zhang
National Institute of Advanced Industrial Science and Technology (AIST), 2-17 Tuskisamu-Higashi, Toyohira-ku, Sapporo 062-8517, Japan

DOI 10.1002/aic.10197
Published online in Wiley InterScience (www.interscience.wiley.com).

Since 2000, a technical program was developed to convert biogas into hydrogen-rich gas, and to demonstrate the possibility of applying the acquired hydrogenous gas to the polymer electrolyte fuel cell (PEFC). The gas conversion was accomplished in two steps, successively, in a desulfurizer that removes the hydrogen sulfide in biogas and in a hydrogen-rich gas producer that converts the desulfurized biogas into hydrogen-rich gas containing CO less than the PEFC-tolerable value of 10 ppm. The gas producer consisted of four catalytic reactors, in succession, a steam reformer, two water-gas-shift reactors, and a selective CO oxidizer. Determining the necessary conditions for all such reactors and the applicability of the produced hydrogen-rich gas to a 50-watt model PEFC stack is examined. Experiments were conducted using clean model biogas over commercial catalysts. A successful production of the PEFC-usable hydrogen-rich gas was fulfilled, and the gas showed a composition of about 70 vol. % H_2, 30 vol. % CO_2, and residual CH_4 (<1.0 vol. %). Directly applying the gas to the downstream model PEFC stack generated stable powers higher than 50 watts, provided the equivalent hydrogen feed was sufficient. Nonetheless, the CO_2 in the gas obviously reduced the stack performance. Compared to the case running on pure hydrogen, the stack exhibited not only a lower voltage (power) at a given current, but also a smaller limit current that restricts the maximal output from the stack at each specified hydrogen feed rate. © 2004 American Institute of Chemical Engineers *AIChE J,* 50: 2467–2480, 2004

Keywords: biogas, hydrogen production, hydrogen purification, polymer electrolyte fuel cell (PEFC), CO_2 poisoning

Introduction

Biogas is becoming an increasingly important and environmental-friendly fuel source, because it usually comes from anaerobic digestion of organic wastes, such as crop residues, animal manure, and municipal sewage (Hammad et al., 1999; Weiland, 2000). The gas contains 50–70 vol. % methane and 30–50 vol. % CO_2, with a few percent of hydrogen, nitrogen and several-thousand-ppm of hydrogen sulfide (Hammad et al., 1995; Huang and Crookes, 1998). Due to the nature of the wide distribution of waste materials, and the difficulty to collect them together, biogas is generally produced through on-site installations of digestion facilities. This makes the gas to be most suitable for isolated energy systems. Shiga et al. (1998) estimated that any other centralized use of biogas might have to require a high cost for gas transportation.

The micro-gas engine may be the most common electricity generator so far used in the isolated power systems fueled with biogas (Neyeloff and Gunkel, 1981; Karim and Wierzba, 1992; Huang and Crookes, 1998;). From the viewpoint of improving energy efficiency, the use of various kinds of fuel cells has also been tested. The earliest effort made was to run the phosphoric acid fuel cell (PAFC) on biogas (Pandya et al., 1988; Ascoli et al., 1989; Naumann and Myrén, 1995). In this case, a gas

Correspondence concerning this article should be addressed to Z.-G. Zhang at z.zhang@aist.go.jp.

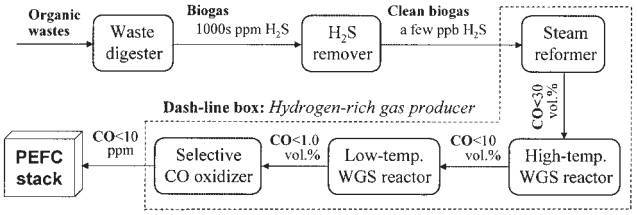

Figure 1. Proposed PEFC system using anaerobic digestion biogas of organic wastes as fuel.

processor was required ahead of the PAFC to clean up the biogas, and to convert it into hydrogen-rich gas. Later, the application of biogas to the solid oxide fuel cell (SOFC) was extensively tested by a British research group through using a model tubular SOFC (Staniforth and Kendall, 1998, 2000). No reforming was made for the gas, because of the internal dry reforming by the coexisting CO_2 (Staniforth and Ormerod, 2002). Most recently, a pilot test applying biogas to the molten carbonate fuel cell (MCFC) was also reported (Bischoff and Huppmann, 2002). Its result was promising, bringing the project now to carry on developing the direct carbonate fuel cell (DFC) driven with biogas.

Since 2000, we have worked on a technical program to convert the biogas from animal manure digestion into hydrogen-rich gas, and to demonstrate the possibility of using the produced hydrogenous gas to cogenerate heat and electricity via the polymer electrolyte fuel cell (PEFC). The livestock farms located in cold northern areas, such as in Hokkaido, Japan, were considered to be the potential customers of the proposed cogeneration system. In Hokkaido, there are many livestock farms, and the animal excrement from the farms are raising serious concerns about the pollutions toward air, soil, and underground water of the area. Environment-friendly treatment of excrement has, therefore, been officially required. In response to this, the anaerobic digestion of cattle manure is going to be popular in Hokkaido and several demonstration plants are already in operation. However, this area needs house heating and hot water for more than 6 months in every year, due to the cold weather. With all of these recognitions, we proposed the use of the PEFC to cogenerate heat and electricity from manure digestion biogas, and, thereby, started the research program.

Figure 1 shows the proposed system. The digestion facility that provided the research program actual biogas was located in Rakuno Gakuen University (College of Dairy Agriculture), Hokkaido (being built via other national projects). The gas conversion was fulfilled in two successive steps, first by a desulfurizer removing the biogas-contained H_2S to ppb levels, and then by a hydrogen-rich gas producer, that is, the boxed part in Figure 1, that makes the desulfurized clean gas into hydrogenous gas, with CO less than the PEFC-tolerable value, say, 10 ppm in this work. The first step of desulfurization is critical to avoiding the downstream poisoning of catalysts and PEFC from sulfuric species. The hydrogen-rich gas producer consisted of four catalytic reactors, in succession, a steam reformer, two water-gas-shift (WGS) reactors operated at, respectively, a high and a low-reaction temperature, and a selective CO oxidizer. Without removal of its CO_2 and CH_4, the hydrogen-rich gas from the producer was fed to the PEFC stack directly. Figure 1 also mentioned the possible CO concentrations at each reactor exit, which were decided according to the tests of Zhang et al. (2002) and Effendi et al. (2002) using micro-quartz reactors.

This article is about the hydrogen-rich gas production from desulfurized biogas. By using gas mixtures of CH_4 and CO_2 to simulate the H_2S-removed clean biogas, the major conditions for the four involved catalytic reactions were examined. Commercial catalysts were employed for the examination so as to ensure the acquired data immediately applicable to the technology development. A 50-watt model PEFC stack was tested by running it on the produced hydrogen-rich gas, with an aim of predemonstrating the applicability of the gas to PEFC, and the stability of the proposed system in Figure 1.

Experimental

Hydrogen-rich gas producer

Figure 2 shows the makeup of the tested hydrogen-rich gas producer. Instead of being a compact gas processor, the producer was simply a test apparatus that combined all the involved reactors and other necessary parts, such as steam generation and measurement. For each of the reactors, independent feed lines, as well as sampling ports, were designed to allow independent operation required for testing its reaction conditions. A more detailed description was given in a previous article (Zhang et al., 2004).

The producer consisted mainly of four fixed-bed reactors: a steam reformer (RFMr), a high-temperature WGS reactor (HTSr), a low-temperature WGS reactor (LTSr), and a selective (preferential) CO oxidizer (PROXr). Of REMr and HTSr, each had a steam generator (SGr). Water was fed to SGr via a water pump (WP) from a water tank (WT). The generated steam was carried into RFMr by the model biogas formed with mixing CH_4 and CO_2 from their respective cylinders, and into HTSr by the reformate after RFMr. Before PROXr, a naturally cooled water trap was installed to remove most of the steam in the reacted gas from LTSr. Then, oxygen was added to the dewatered gas from a cylinder via a mass-flow meter to provide the oxidant for the PROX reactions. A gas of argon blended with 10 vol. % H_2 was used to reduce the catalysts in all the reactors.

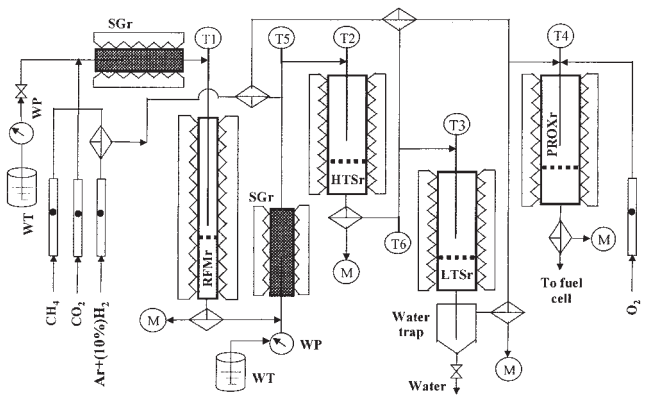

Figure 2. Hydrogen-rich gas producer for producing PEFC-adaptive hydrogenous gas from desulfurized clean biogas.

Table 1. Reactors and Their Catalysts Used to Produce Hydrogen-Rich Gas from Desulfurized Biogas (Clean Model Biogas in the Work) for a 50W Model PEFC Stack

Reactor	Size [mm][(1)] (SUS-made)	Used Catalyst					
		Comp.	Shape	Size [mm]	Bulk Density [kg/m^3]	BET Surface [m^2/g]	Meso[(2)] Pore Size [nm]
RFMr	$14.9\phi \times 820$L	Ni/Al_2O_3	Sphere	3.0ϕ	970	1.9	3.4–38.5 (7.8)
HTSr	$24.8\phi \times 570$L	Fe/Cr-base	Cylinder	$9.5\phi \times 4.8$	920	73.6	1.6–38.5 (30.4)
LTSr	$24.8\phi \times 570$L	Cu/Zn-base	Cylinder	$3.2\phi \times 3.2$	1300	50.3	1.6–38.5 (12.4)
PROXr	$24.8\phi \times 630$L	Ru/Al_2O_3	Cylinder	$3.3\phi \times 3.5$	950	92.9	3.2–38.5 (6.8)

(1) "L" indicates the length of heated section of reactor. For reactor, "ϕ" means inner diameter.
(2) The value in parentheses shows the size of pores with the highest pore volume fraction.

All the reactors were stainless-steel-made pipes, and their sizes are specified in Table 1. These sizes were particularly chosen according to the preliminary tests of Zhang et al. (2002) in small quartz reactors, so that the new apparatus was able to produce hydrogen-rich gas from biogas at rates up to 2.5 L/min. The reactors were electrically heated, by either a jacket furnace (for RFMr), or by electric wires that are wrapped around the reactor (for HTSr, LTSr & PROXr). In each reactor, a sintered porous plate was mounted at a position of 30–50 mm below the middle point of the heated section to support the catalyst. Thermocouples of 1.5 mm in dia. (T1 to T4) measured the temperatures inside the reactors, and PID controllers controlled the temperatures. Being aware of the highly endothermic feature of RFM, the thermocouple in RFMr was located about 10 mm above the catalyst support to measure, and, additionally, to control the possibly lowest reaction temperature. Against this, the reactions in the other reactors are more or less exothermic and, thus, had their temperature measurements usually at the center of the catalyst beds. That is, their measuring positions were adjusted in accordance with the loaded catalyst amounts. Two SGrs were stainless-steel-ball packed stainless steel pipes of 24.8 mm in I.D. and 200 mm in length. Each of them was heated with a jacket tape heater, and the power for the heater was adjusted to guarantee the evaporator outside-wall temperature (measured with thermocouple) not over 523 K. The reactor and SGrs were connected via 1/4-inch stainless steel pipes. All pipes down to the water trap after LTSr were warmed (373 to 403 K) with tape heaters to prevent steam from condensation. The thermocouples T5 and T6 were actually two monitors for such temperatures along the pipelines.

Mass-flow meters controlled the flows of involved feedstock gases. Each of the two SGrs was equipped with a high-pressure liquid pump to send water, and also to measure the water amount. The reacted and reactant gases were analyzed in a two-channel micro-TCD gas chromatograph (P200H, Agilent Technologies) to determine the dry-base molar concentrations of gas components H_2, CO, CH_4, and CO_2. For this, a micro-suction pump was employed to create a sampling flow of 50 mL/min, and to make the measurement possible for all the reactors, even during continuously running the entire producer.

The adopted commercial catalysts are characterized in Table 1. The first three were so far commonly used for the same reactions, as Ni/Al_2O_3 for CH_4 reforming, Fe/Cr and Cu/Zn for WGS, at high and low-reaction temperatures, respectively. The fourth contained 0.5% Ru, and was conventionally used for hydrogenation until recently being tested for selective CO oxidation (Oh and Sinkevitch, 1993; Tabata, 2000). Concerning these catalysts, we may find many literature studies, but few of them would be really done, as in this article, over industry-type catalysts and in metal-made large-size reactors.

The test for the producer was begun with raising the temperatures of the reactors under an Ar-H_2 (10 vol. %) flow of 100 mL/min. In order to prevent the catalyst from being overheated, the temperature increasing speed was always lower than 100 K/h. For RFMr, the catalyst reduction proceeded along with the temperature rise, up to the reaction temperature of 1063 K, whereas, for the other reactors, this was done via first heating the catalyst to a temperature that was higher than the reaction temperature, and then keeping it there for 1 h. The stated higher-temperature was 533 K for LTSr, and 673 K for both HTSr and PROXr. In these latter cases, naturally cooling the catalysts to their respective reaction temperatures was then executed. The formal reaction test was finally started via the flow switch from Ar-H_2 to feedstock. In this article, the reaction test was conducted first for individual reactors to determine their suitable reaction conditions, and then for the entire producer by running all reactors at once. Therefore, the gas mixtures of H_2, CO and CO_2 were necessarily employed in some cases to model the feedstock gases for HTSr, LTSr, and PROXr.

The tested model biogas was made of 60 vol. % CH_4, and 40 vol. % CO_2 (except for what will be seen in Figures 14 and 15), by taking the average of the possible CH_4 concentrations in realistic biogas (50–70 vol. %).

Model PEFC stack

The tested fuel cell was a 50-watt model PEFC stack made of 22 cells (from a Japanese battery company). Each of the cells had pure platinum electrodes in areas of 25 cm^2. Compared to RtRu electrodes, pure Pt anode is more sensitive to the CO residual in hydrogenous fuel, and very suitable for evaluating the CO removing capability of the proposed Ru-catalyzed PROX. A particular feature of the stack used is that the output characteristics of each cell can be monitored in parallel to those of the stack. This enabled a precise judgment of the stack's running status according to the performances of both individual cells, and of the entire stack. The whole stack was judged to work normally only when each of its cells was not abnormal.

The operation of the model PEFC stack is the same as operating any other PEFCs. Two hot-water bubblers at compliance temperatures of 345 and 355 K were used to humidify the gases entering the anode and cathode gas chambers. The stack temperature, around 353 K in this work, was maintained via a pumped hot-water circulation, and was measured via two

thermocouples at two particularly designated ports. A galvanostat regulated the current passing through the stack, and also measured the stack voltage. The output voltages from the stack and each cell were monitored online using a 30-channel recorder. In response to changing the fuel cell current, the stack temperature varied substantially. The larger the current passing through the cell, the higher the stack temperature came to be, because of the greater heat release from the larger H_2 oxidation (electrochemically). Additionally, the lower electrochemical efficiencies at higher currents would also lead to higher-heat production, and then make the stack temperature higher. The temperature of the circulated water was, thus, correspondingly lowered to counteract the increased reaction heat, and to maintain the stack temperature constant.

Nitrogen was used as a purge gas for the fuel cell test. The test was started with raising the temperatures of water bubblers and fuel cell stack. Purge gas was then sent to both the anode and cathode sides at instructed rates for at least 5 min. The cells started to work as the flow was switched from purge gas to oxygen for the cathode, and to fuel gas for the anode. The stack was run first at the open-circuit state for more than 30 min until the current was imposed to start the measurement. Pure oxygen, instead of air, was used as an oxidant in the work, because the used bubblers were smaller, and could hardly afford the high flow rate of air. The performance of the model PEFC stack was examined first with pure-hydrogen fuel. By blending CO_2 and CH_4 into pure H_2, the influences of two such alien gas species were also investigated. The flows of oxygen and all gas components for the simulated hydrogen fuels were controlled using mass-flow meters, whereas the rate of the hydrogen-rich gas produced from model biogas was measured with a gas meter between the gas producer and the cell stack.

Results and Discussion

Individual reactors

The necessary conditions for the reactions occurring in RFMr, HTSr, LTSr, and PROXr were examined in the following. The stated conditions include reaction temperature, space velocity (*Sv*), steam-to-gas ratio (**for former three**), and oxygen-to-CO ratio (for PROXr). The space velocity refers to the gas volume flowing through one-gram catalyst in 1 h. It was calculated usually on dry base (subscript: "dry") at 273 K, and the atmospheric pressure (subscript: "st"). By treating the model PEFC stack as a reactor, the section also included the test of running the stack on pure H_2, and the H_2 blended with CO_2 and CH_4.

Steam reforming (RFM). Methane conversion is the criterion for choosing the conditions of RFM. Thermodynamic calculation (Chawla and Ghosh, 1992), as well as the experimental result of Effendi et al. (2002), demonstrated that the reaction temperature should be higher than 1023 K, for achieving CH_4 conversions higher than 98%. This is generally known for CH_4 steam reforming, and here we, thus, had no test for the reaction temperature T_{RFM}, by taking a slightly higher one 1063 K as the operating temperature for RFM.

The size of catalyst is greatly influential to the gas diffusion processes during reaction. Consequently, the employed industrial Ni/Al_2O_3 catalyst may require different space velocity, and steam-to-methane (Steam/CH_4) ratio for realizing the same CH_4 conversion as the other fine catalysts can provide. Figure 3 shows the relevant result obtained. From the data for 4.5- and 6.0-g catalysts, we can see that to ensure 98% CH_4 conversion, the highest allowable $Sv_{st,dry}$ was about 10,000 mL/(g h). This is a value much lower than many others found in literature, such as in Zhang et al. (2002) and Effendi et al. (2002), for fine (pulverized) catalysts. A worse result was shown in Figure 3 for the catalyst load of 3.1 g (□). The conversion at each specified $Sv_{st,dry}$ was evidently smaller than those for 4.5 and 6.0 g catalysts, whereas the decrease of the conversion with raising $Sv_{st,dry}$ was also quicker. Since no obvious difference was identified between the two former cases, such results may indicate that, for our reactor, the catalyst amount of 3.1 g was too small to avoid a pronounced configurational effect arisen from the catalyst support. Near the catalyst support, the contact and impaction between catalyst particles and reactant gases are less efficient than in the bulk reaction zone, because some "dead" corners or ports always exist in the vicinity of the support plate. The share of the dead corners decreases as the catalyst load increases, and, when the load is over a certain value, say, 4.5 g in Figure 3, it would become negligible to cause very little effect of catalyst amount on the conversion at the same $Sv_{st,dry}$.

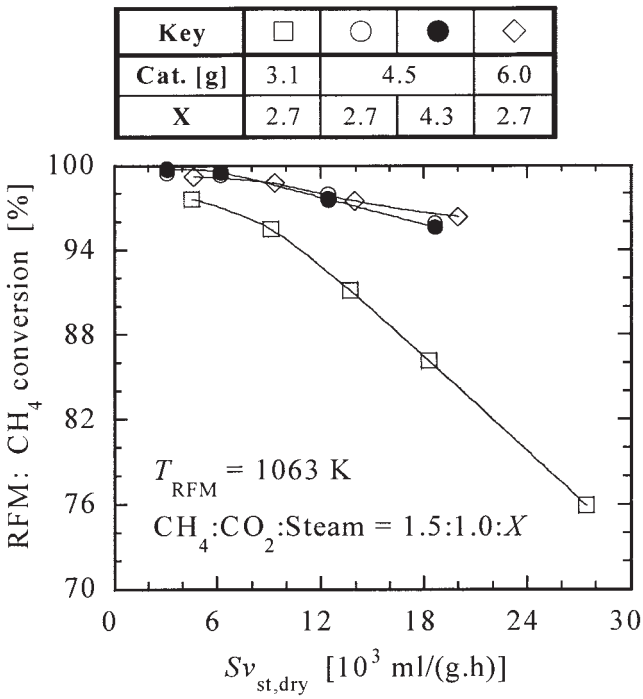

Figure 3. Variations of methane conversion with space velocity and steam ratio in reforming reactor (RFMr).

For the 4.5 g catalyst load, the CH_4 conversion exhibited little variation, also with the change of Steam/CH_4 ratio from 2.7/1.5=1.8 to 4.3/1.5=2.9. The result agrees with the observation of Zhang et al. (2002) for fine Ni/Al_2O_3 catalyst, who found that the CH_4 conversion quickly increased with increasing the steam feed, but the quick increase stopped when the Steam/CH_4 ratio became higher than 0.7. Nonetheless, there might be another necessary condition for the observed little effect of steam ratio on CH_4 conversion. This is about the reaction conditions (mainly $Sv_{st,dry}$), which should be con-

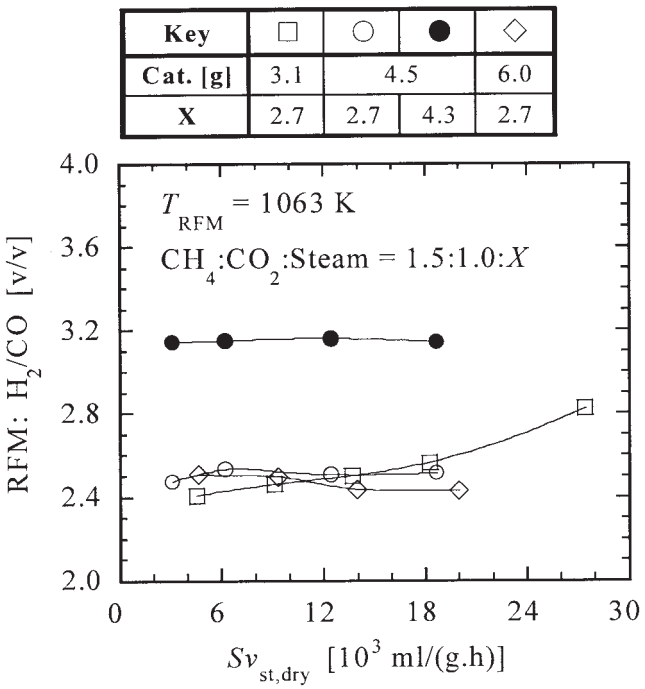

Figure 4. H_2/CO molar ratio of the reformate from reforming reactor (corresponding to Figure 3).

trolled to allow the CH_4 conversions over, such as 95%. Otherwise, the Steam/CH_4 ratio would affect the reforming reactions, and in turn, the CH_4 conversion.

The aforementioned change of Steam/CH_4 ratio, however, greatly varied the composition of the gas from RFMr, as is shown in Figure 4, where the hydrogen-to-CO (H_2/CO) ratios for the same tests in Figure 3, were plotted. The H_2/CO ratio was obviously higher at the higher Steam/CH_4 ratio of 4.3/1.5 (●), and, for all the $Sv_{st,dry}$ tested, it was above 3.0. For the steam reforming of methane, the theoretical H_2/CO ratio is 3.0 (Eq. A1). When CO_2 is present in the feedstock, the CO_2 reforming may simultaneously take place to give a theoretical H_2/CO ratio of 2.0 (Eq. A2). Therefore, with the two CH_4 reforming reactions, only the H_2/CO ratio should be between 2.0 and 3.0. The measured values in excess of 3.0 indicated then some other reactions that converted CO to H_2, along with CH_4 reforming. An important one is the water-gas-shift (WGS, Eq. A3). Over a dispersed NiO/MgO catalyst Choudhary et al. (1998) reported an obvious WGS, along with CH_4 reforming. Then, Figure 4 clarifies that for RFM, the increase in the steam ratio greatly enhanced the simultaneous WGS. At the lower steam feed of Steam/CH_4=2.7/1.5, the H_2/CO ratios were all around 2.5, regardless of the catalyst load. It reveals then a weakened WGS, compared to that for another higher Steam/CH_4 (4.3/1.5), actually showing a predominant determination of steam ratio on the simultaneous WGS, and on the value of H_2/CO.

Furthermore, combining Figures 3 and 4 shows that the H_2/CO ratio was likely to vary little with CH_4 conversion when the conversion was higher, such as over 96 vol. %. In a wider range (□ in Figure 4), however, the ratio slightly increased with decreasing the CH_4 conversion. Essentially, this indicates a slightly higher proportion of CO converted to H_2 at the lower CH_4 conversion, and two causes can be considered for this. First, at the lower CH_4 conversion, the share of CO_2 reforming is perhaps smaller so that the percentage of steam reforming is larger to give, thus, a higher overall H_2/CO ratio. Second, there may be a higher proportion of CO converted to H_2 via WGS once the CH_4 conversion is lower. In theory, the latter cause sounds particularly plausible, because at the lower CH_4 conversion there is more steam left in RFMr to facilitate WGS. The lower conversion of CH_4 implies less formed CO, but this would not decrease much of the percentage of CO converted by WGS, because the reaction rate of WGS is fast at 1063 K to make the reaction proceed always according to equilibrium. Thus, the little varied H_2/CO ratio at higher CH_4 conversion (>96%) should be due to little room left for varying the amount of steam after RFM.

In addition, it was found that the lowest steam ratio required for reforming the examined biogas without any loss in catalyst activity was around Steam/CH_4=1.8. At such a steam ratio, the CO concentration in the reformate gas was usually around 27 vol. %. This value is between the theoretically predicted highest CO fractions of 25 vol. % for steam reforming, and 50 vol. % for CO_2 reforming, corroborating the simultaneous occurrences of the two reactions.

Water-gas-shift (WGS). Both HTS and LTS refer to the same reaction WGS; they are thus examined together in the following. A presumption made for the examination is that the same catalyst amount is used for the two reactions to ensure the nearly same space velocity. As a matter of fact, the WGS reaction (Eq. A3) does not vary the wet-gas volume, although it slightly increases the dry-gas volume.

The reacted gas from RFMr was used as the feedstock of HTSr, and in turn of LTSr. This made it impossible to measure the flow rates of dry gas and unreacted steam after RFMr, but they are needed for estimating the space velocities and steam ratios in HTSr and LTSr. For this, the Eqs. A7 and A8 in the Appendix were developed to, respectively, formulate the post-reaction dry-gas flow rate, and reacted steam amount in unit time for a reaction system, consisting of reactions A1 to A4. The equations are commonly applicable to RFM, HTS, and LTS. Thus, the space velocities, and steam, or oxygen ratios stated hereafter for the reactors other than RFMr, are all the computed values under the involvement of Eqs. A7 and A8.

Figure 5 shows the dependences of the outlet CO concentration of HTSr on reaction temperature (T_{HTS}) and steam ratios (volumetric) toward both inlet dry-gas (steam/gas) and inlet CO (steam/CO). The feedstock gas was from an RFM operation at steam/CH_4=1.8, which thus led to possibly the highest CO content around 27 vol. % for the reformate of biogas. Three-temperatures T_{HTS} were tested at a given dry-gas space velocity $Sv_{st,dry}$ of 1060 mL/(g h), under a given catalyst load of 71.0 g.

For a given steam ratio, the outlet CO in Figure 5 obviously decreased with raising T_{HTS} from 653 to 703 K, where there was not much difference detectable between 703K and 743 K. Hence, the WGS reaction over the tested commercial Fe/Cr catalyst is kinetically controlled below 703 K, whereas above this temperature the thermodynamic control would be predominant. This clarifies that the optimal T_{HTS} for the catalyst should be around 703 K. At 703 K, the outlet CO manifested pronounced decreases along with the increase of steam/gas ratio from 0.75 to 1.25 v/v. However, further increasing the steam

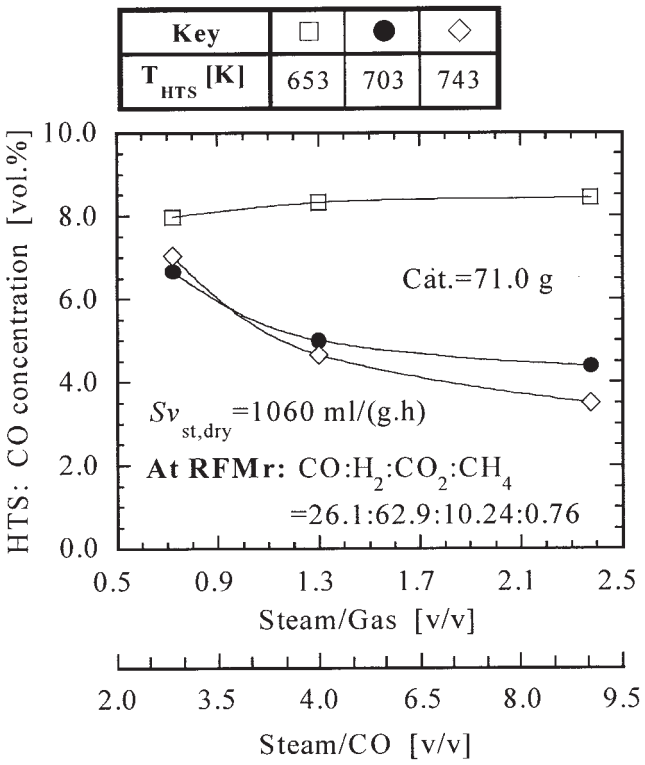

Figure 5. Dependences of high-temperature water-gas-shift (HTS) reaction on steam ratio and temperature.

ratio had caused little improvement on the CO abatement. Examining the data at T_{HTS}=743 K, one can see the similar variation of the outlet CO with steam/gas ratio. Thus, the least steam/gas ratio for HTS over the tested catalyst should be about 1.2 v/v, giving a corresponding steam/CO ratio around 4.0 v/v. Nonetheless, it is questionable if such a steam/CO ratio is generally applicable to other feedstock with less CO. Less CO requires less steam feed and, thus, the steam/gas ratio must be smaller than the required value of 1.2 v/v.

At the lower T_{HTS} of 653 K, the dependence of HTS performance on the steam ratio differed from the aforementioned. The outlet CO in this case slightly ascended with raising the steam/gas ratio. Enlarging the steam feed has two competitive effects on WGS. One is to increase the reaction rate and shift the equilibrium to the right to result in less CO in the outlet stream, and the other is to reduce the reaction time via increasing the wet-gas space velocity to raise the outlet CO. Of them, the latter effect is dominant at lower T_{HTS} for the kinetically controlled situation, until it finally surrenders to the former at higher T_{HTS}, where the reaction becomes sufficiently fast. Responding to this, the outlet CO in Figure 5 possessed opposite variations with steam/gas ratio at T_{HTS}>703 K and T_{HTS}=653 K. Nonetheless, the influential degree of steam ratio on outlet CO was commonly lower at higher ratios, revealing a gradually decreased sensitivity of WGS toward steam amount.

There was a cross between the curves for 703 and 743 K in Figure 5. At lower steam ratios, the concentration of outlet CO was larger for the case of 743 K, whereas, at higher steam/gas ratios, it was reversed to be larger at 703 K. These results might be interpreted in terms of the thermodynamically and kinetically controlled WGS reactions, respectively. Hence, in addition to the temperature, the steam amount may change the rate-controlling factor of WGS, as well. When T_{HTS}>703 K, Figure 5 shows that a change of the controlling factor from thermodynamic to kinetic ones might occur as the steam/gas ratio was increased up to 1.0.

Figure 6 shows a similar test for LTS by employing the gases from HTSr at 653 K shown in Figure 5 as the feedstock. Thus, the inlet gases had nearly the same CO fraction of 8.0 vol. %, but different steam contents. These different steam contents formed just the steam ratios for the LTSr inlet plotted in Figure 6. The figure displays also the corresponding steam/gas ratios at the HTSr inlet on account of the fact that the steam ratio for LTSr is not independent. Similar to the analysis made for Figure 5 about HTS, Figure 6 reveals that the suitable temperature for LTS (T_{LTS}) is between 483 and 523 K. Above 523 K, the reaction thermodynamics came into effect, causing the outlet CO to inversely increase with raising T_{LTS}. For T_{LTS} from 483 to 523 K, the left steam after HTS appeared enough to carry on the LTS reaction. This would be the case even when the original steam feed to HTSr, such as at steam/gas = 0.75 v/v in Figure 5, was insufficient to HTS. Thus, the suitable steam ratio for WGS might be determined by considering only HTS without recourse to LTS.

Shown in Figure 7 are the dependences of HTS and LTS reactions on dry-gas space velocity $Sv_{st,dry}$. These tests were

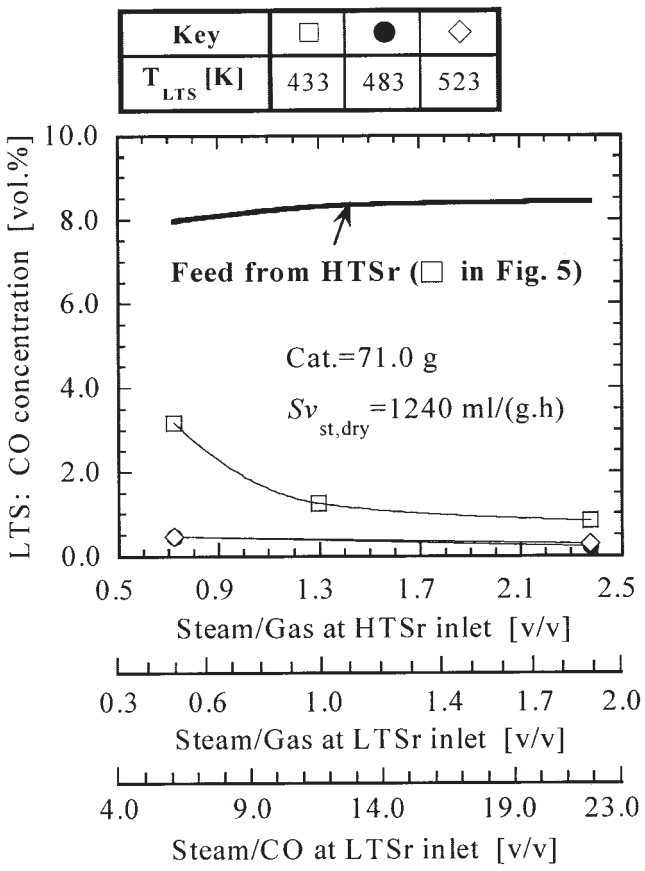

Figure 6. Dependences of low-temperature water-gas-shift (LTS) reaction on steam ratio and temperature (the feed from HTSr directly).

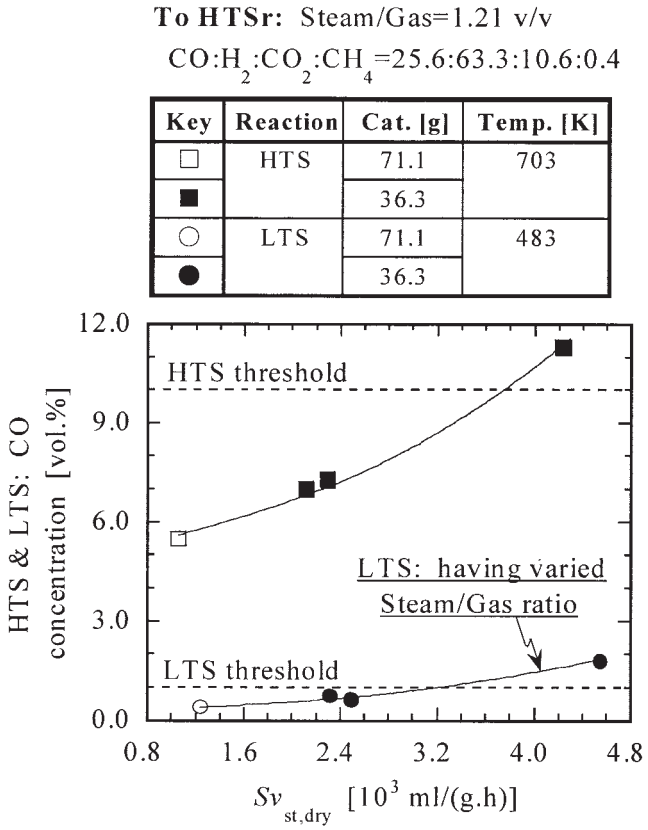

Figure 7. Influence of space velocity on high- and low-temperature water-gas-shift reactions (the outlet gas from HTSr being used as the feedstock of LTSr).

conducted at the earlier-chosen suitable steam/gas ratio for HTS (1.21 v/v), and temperatures for both (703 K and 483 K). Two reactions were tested via a single feedstock to HTSr. The criteria adopted to determine the suitable space velocities of HTSr and LTSr are their threshold values of CO concentration generally suggested. That is, the CO content should be reduced to less than 10 vol. % through HTS, and less than 1.0 vol. % via LTS. Then, Figure 7 demonstrates that the necessary $Sv_{st,dry}$ should be lower than 3,500 and 3,200 mL/(g h) for HTSr and LTSr, respectively. These two values are much lower than the data reported by Zhang et al. (2002) for the same catalysts, but finer, showing again a great effect of catalyst size on catalytic activity.

Preferential CO oxidation (PROX). The test for the selective CO oxidation used the gas mixtures of H_2, CO_2 and CO as feedstock. To simulate the hydrogen-rich gas from LTSr (composition being in **Figure 13**), the mixtures had basically 70 vol. % H_2, 30 vol. % CO_2, and CO less than 1.0 vol. %. The mixtures were also humidified through a water bubbler at room temperature, noting that in Figure 2, the process hydrogen-rich gas was dewatered in a trap naturally cooled.

Figure 8 shows the CO concentration after PROX (left Y, ■●) over 10-g commercial 0.5%Ru/Al_2O_3 catalyst at a $Sv_{st,dry}$ of 4250 mL/(g h) under reaction temperature (T_{PROX}) varying from 343 to 463 K. The atomic ratio of oxygen to CO (O/CO) was 1.1, and the inlet CO concentration had two different values, 0.48 and 0.93 vol. %. For both the tested inlet CO concentrations, with increasing temperature T_{PROX}, the outlet CO first decreased and then increased until it decreased again at higher T_{PROX}. Decreasing of the outlet CO with rising T_{PROX} was ordinarily quick, especially at T_{PROX}>423 K. In-between, the speed of increasing was faster when the inlet CO concentration was higher. For the 0.48 vol. % inlet CO, the increase was very slight at T_{PROX} from 363 to 423 K (annotated by dotted lines). Furthermore, the figure shows that in both the tested cases a local bottom concentration of outlet CO appeared at about 383 K.

Accompanying with the earlier CO evolution, the formed CH_4 (right Y, □○) progressively increased with raising T_{PROX} after it became detectable at about 385 K. Below 423 K, the outlet CH_4 fraction was low, such as smaller than 0.1 vol. %, but the increasing temperature since then considerably accelerated the CH_4 evolution. Methane was formed from methanation of CO and CO_2. The former promoted CO removal, which was responsible for the quickly decreased outlet CO at T_{PROX} >423 K. If the selectivity of methanation toward CO were high, it would bring a huge benefit to PROX. The actual result, however, is that the formed CH_4 was usually much more than the reduced CO. For example, in Figure 8, the reduction of the outlet CO from 0.27 to 0.12 vol. % was accompanied by a methane formation of about 0.4 vol. % (see ■□). Therefore, for PROX, the simultaneous methanation is at all not expected, implying that T_{PROX} must be lower than 423 K so as to avoid the substantial CH_4 formation.

Surely, the decrease of the outlet CO with raising T_{PROX} below 383 K is due to the correspondingly increased kinetic

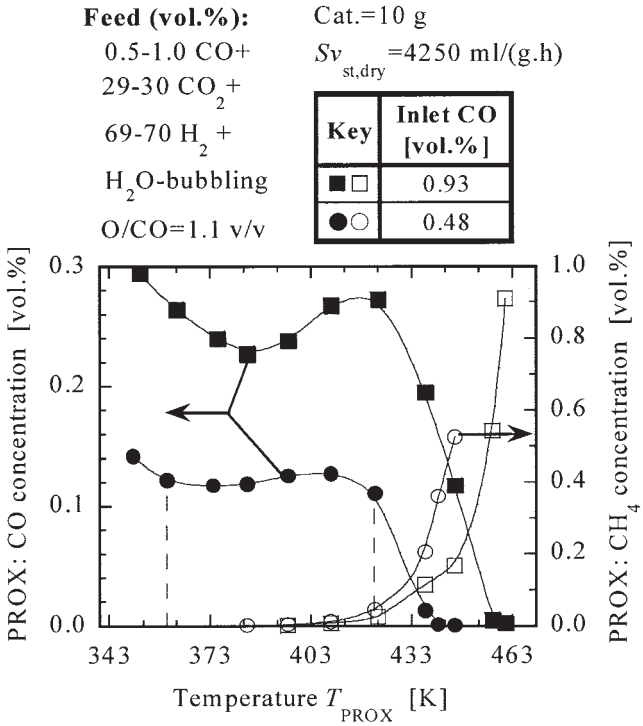

Figure 8. Temperature window for preferential CO oxidation (PROX) over the 0.5%$Ru/A1_20_3$ catalyst (simulated LTSr's outlet gas being used for the test)

rate of CO oxidation. Meanwhile, the increase in reaction temperature reduced the priority of CO adsorption onto the catalyst surface, which decreased the CO oxidation and left more oxygen to react with hydrogen. The competition between two such actions (kinetic rate increase vs. selectivity decrease) created, thus, the minimal outlet CO around 383 K, indicating an optimal T_{PROX} of about 383 K for the tested catalyst. Nevertheless, the coexisting CO methanation showed us an alleviated deterioration in CO removal at T_{PROX} beyond 383 K. Until the methanation became substantial at 423 K, the methanated CO actually counteracted the partial decrease of CO removal with raising T_{PROX}, so that the outlet CO remained insensitive to temperature in a wide range of T_{PROX}, say, between the two dotted lines in Figure 8. This essentially extended the temperature window of PROX, at a cost of CH_4 formations less than 0.1 vol. % making, thus, the suitable T_{PROX} for the tested Ru/Al_2O_3 catalyst be wider from 373 to 423 K, rather than be at 383 K only.

The CH_4 formation was faster at lower inlet CO. Shown in Figure 8, this gives the case of 0.48 vol. % inlet CO (○) both an earlier detection of the formed CH_4, and a higher outlet CH_4 fraction at each temperature tested. At a higher inlet CO concentration, there is more CO available for covering the catalyst surface, leading to fewer active sites for H_2 adsorption and dissociation, and, in turn, the less methanation of CO and CO_2. VanderWiel et al. (1999) had pointed out that the occurrence of CO methanation necessarily requires the dissociation of molecular hydrogen.

Figure 9 serves to determine the necessary space velocity and O/CO ratio for abating inlet CO (<1.0 vol. %) down to less than 10 ppm via PROX over the tested Ru catalyst. The plotted data were for three different velocities $Sv_{st,dry}$ and successively changed O/CO ratios. All examined temperatures were within the range chosen earlier. From the outlet CO concentration in Figure 9a, we can see that the inlet CO (<1.0 vol. %) can surely be lowered to less than 10 ppm at $Sv_{st,dry} \leq 4250$ mL/(g h). Correspondingly, the required O/CO ratio should be around 2.3 v/v for the highest inlet CO fraction of 1.0 vol. %. At $Sv_{st,dry}$ = 8,500 mL/(g h), it seems possible to oxidize CO down to the desired 10 ppm at an O/CO ratio of 2.5 v/v, when the inlet CO is less than 0.5 vol. %. The CO oxidation to the same extent appeared achievable also for the inlet CO of 1.0 vol. %, but the O/CO ratio should be substantially high, say, up to 3.0 v/v. Hence, the larger the inlet CO concentration and space velocity are, the higher the required O/CO ratio must be for lowering the supplied CO down to the same low level. Snytnikov et al. (2003) had reported a similar effect of inlet CO on the required O/CO ratio. In our case, these results revealed that the appropriate space velocity $Sv_{st,dry}$ should be smaller than 8,000 mL/(g h, so that the inlet CO up to 1.0 vol. % can be surely oxidized down to 10 ppm at O/CO<3.0.

Figure 9b shows the CH_4 formation corresponding to Figure 9a, clarifying again that more CH_4 was formed at higher-temperature and lower inlet CO concentration. Furthermore, it shows that, at T_{PROX}<420 K, the formed CH_4 in PROX was less than 1,000 ppm for the generally encountered gases from LTSr, which may have CO around 0.5 vol. %. At the other lower T_{PROX} near 393 K, and higher inlet CO contents up to 1.0 vol. %, the formed CH_4 was rather less, such as lower than 500 ppm. The CH_4 formation also increased with increasing the O/CO ratio for each given inlet CO. This should be still subject

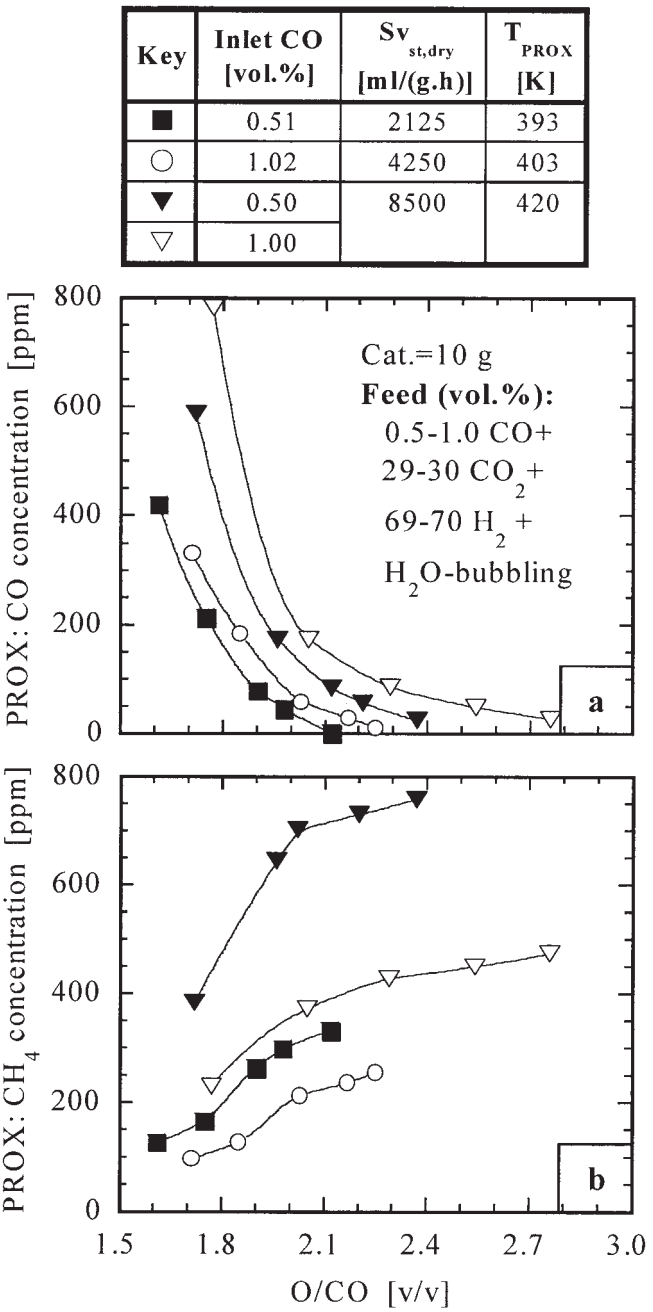

Figure 9. Necessary space velocity and O/CO ratio for selectively oxidizing CO down to less than 10 ppm (simulated LTSr's outlet gas being used for the test).

to the CO coverage, which is lower at higher O/CO ratio when more O_2 is supplied to oxidize more CO to free more catalyst sites available for the H_2 dissociation, and then methanation. Besides, the formed CH_4 was found to be more at lower-space velocity $Sv_{st,dry}$, due to the longer reaction time, but this appeared much less important compared to the decreased O/CO ratio required for removing CO down to 10 ppm at the lowered $Sv_{st,dry}$.

Model PEFC stack. Figure 10 shows the voltage (left Y) and power (right Y) outputs of the 50-watt PEFC stack run on

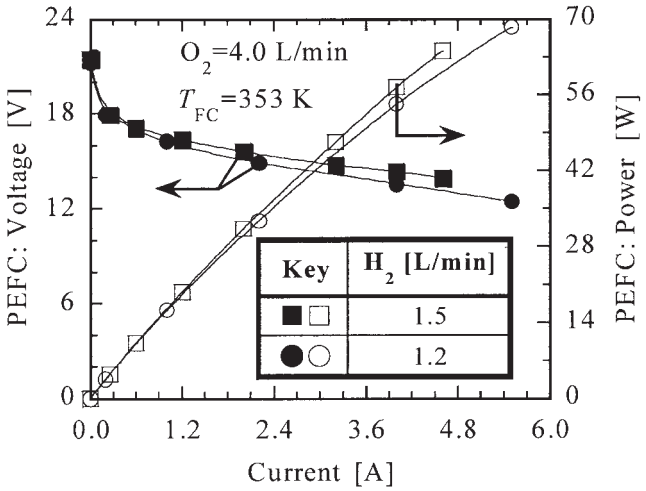

Figure 10. Performance of the 50W model PEFC stack run on pure-hydrogen fuel.

pure hydrogen. Two hydrogen feeding rates 1.2 and 1.5 L/min, were examined under a given oxygen supply of 4.0 L/min. The stack had an open-circuit voltage of about 21.5 V, indicating an average open-circuit voltage of 0.977 V for each cell. However, the output voltage from every single cell differed slightly from one to one. For our stack, the difference was about ± 0.04 V, and it persisted in the fuel cell tests, such that any abnormal performance of the stack was observed to start always from one or a few of the specific cells. Thus, all the data presented here for the stack implied a fact that each of the cells had normally worked.

From Figure 10, we can see that, for pure-hydrogen fuel, the feed of 1.2 L/min is surely enough to generate the desired power of 50 W (voltage: 14.0 V, current: 3.6 A). In fact, a power up to 70 W was achieved at this H_2 feeding rate (●○). Raising the H_2 rate to 1.5 L/min had caused the stack rather higher outputs in voltage and power at each given current (□■). This may indicate that the H_2 rate of 1.2 L/min might be very close to the least fuel feed required by the stack. The off-gas flow from the stack running on 1.2-L/min pure H_2 was, thus, measured to verify the judgment. It was found that 56% and 87% of the supplied H_2 were consumed for the power outputs of 50 and 70 W, respectively. On the basis of these, the fuel cell tests hereafter adopted the hydrogen feed rate of 1.5 L/min in examining the possible loss of performance by blended CO_2.

Figure 11 shows the variations of stack voltage and power outputs with gradually increasing CO_2 content in hydrogen fuel. The measurement was made at a current of 4.0 A, so that the power output could be near 50 W. It is evident that the presence of CO_2 in fuel gas significantly reduced the cell performance. The higher the CO_2 fraction in the gas, the larger the performance loss was. This CO_2-induced performance loss for fuel cell had been earlier reported in several works for anodes (Dhar et al., 1986; Wilson et al., 1993), and for single cells (de Bruijn et al., 2002; Ball et al., 2002). As regards to our tested PEFC stack, Figure 11 shows that the voltage output decreased from 14.4 to 13.3 V, indicating a power reduction from 57.5 to 53.2 W, with increasing the CO_2 fraction from 0 to 36 vol. %. At a given CO_2 fraction, the performance reduction was found to be considerable at a higher imposed current, as was similarly observed for cell anode by Wilson et al. (1993), and for single cell by de Bruijn et al. (2002). This caused a great decrease in the maximal allowable current (limit current) and power from the stack. Our stack was actually hard to achieve the 50-watt power output when the feed had H_2 of 1.2 L/min, and CO_2 of more than 30 vol. %. Increasing H_2 feed rate can alleviate such suffering. Figure 11 shows in fact that at the H_2 feed rate of 1.5 L/min, the power output can be readily higher than 50 W, even for a CO_2 intake of 36 vol. %. Accordingly, to ensure the desired 50-watt power generation for the model PEFC stack, the lowest H_2 feed rate should be around 1.5 L/min, when the fuel gas contains CO_2 over 30 vol. %.

With the earlier performance reduction, one may wonder if the stack can have stable outputs in long-time running on gases containing CO_2. A test had demonstrated that as long as the imposed current was not over the cells' limit currents, the stack surely could have stable output. This was also shown in Sishtla et al. (1998) for a single cell, and it will be verified further in Figure 15, by running the model stack on hydrogen-rich gas produced from a simulated biogas for a (relatively) long time. Figure 12 presents an examination on the possible influence of CH_4 present in the fuel gas. Definite CH_4 surely remains in the reformate from methane-based fuels, due to the incomplete conversion of CH_4 in RFMr, and the methanation of CO and CO_2 in the H_2-purification reactor (such as PROXr shown in Figures 8 and 9). In the final hydrogenous gas, the CH_4 fraction may reach a few percents, say, 4.0 vol. % here. Figure 12 demonstrates then that such a residual CH_4 would not greatly reduce the fuel cell performance. However, the presence of CH_4 slightly, but surely decreased the limit current of the cells, although it may be alleviated through increasing the H_2 feed rate.

Two mechanisms were proposed for the influence of CO_2 on PEFC performance. The early study of Dhar et al. (1986) on polarization voltages of a Pt-C anode at temperatures for the alkali fuel cells (AFCs), revealed a great effect from diluting the hydrogen fuel. This diluting effect was then generally recognized until Wilson et al. (1993) stressed a poisoning effect of CO-like species formed via the reverse WGS and CO_2

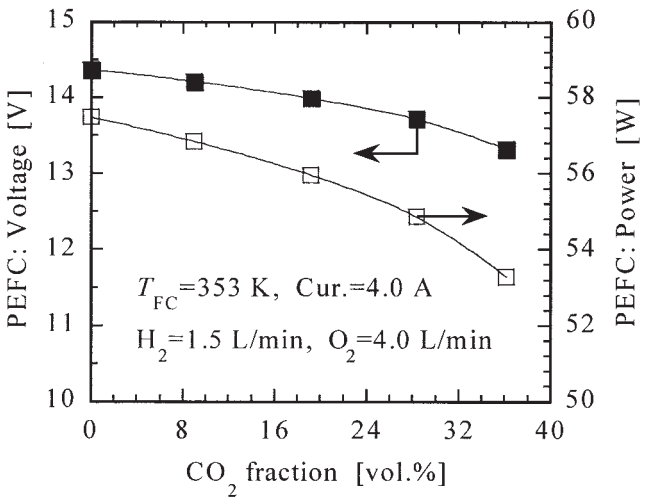

Figure 11. Influence of CO_2 present in hydrogen fuel gas on PEFC performance.

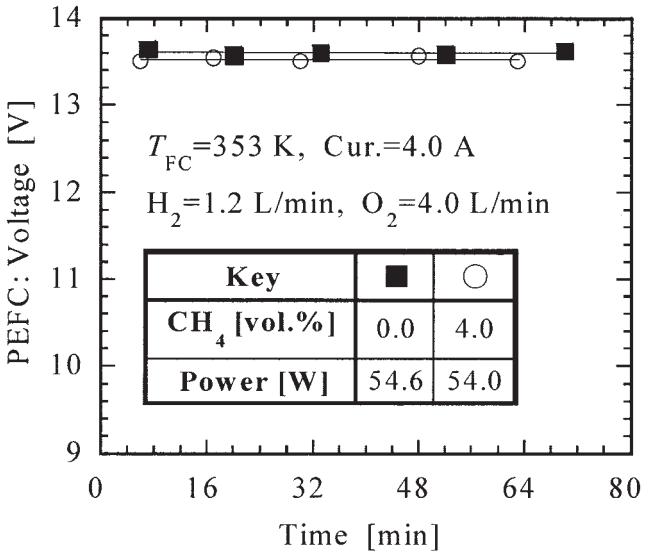

Figure 12. Influence of CH_4 present in hydrogen fuel gas on PEFC performance.

electroreduction over Pt anode, under the PEFC operating conditions. The characteristic of the diluting effect is that the cell performance reduction is linearly correlative with the current density (Dhar et al., 1986). Against this, the poisoning effect likely causes the performance loss to be larger at higher current density (Wilson et al., 1993; de Bruijn et al., 2002). Then, the present results with the model PEFC stack further corroborated two such influential mechanisms. Besides, Figure 11 shows that the magnitude that CO_2 decreases the voltage and power outputs is gradually larger as the CO_2 fraction becomes higher, and the tendency is especially evident at CO_2 fractions above 20 vol. %. While the result may indicate again the presence of the CO_2 poisoning effect, it also reveals that the poisoning effect would be particularly significant when the CO_2 fraction is higher than 20 vol. %. At other smaller CO_2 fractions the diluting effect might be predominant since the cell performance degraded almost linearly with raising the CO_2 fraction. For CH_4, only the diluting effect is active; its lower content (<4.0 vol. %) induced only a slight loss in cell performance. Lifting H_2 feed rate allows more H_2 to be left after the cell reactions, which actually reduces the CO_2 or CH_4 fraction on the anode surface. As a consequence, there should be certainly a suppressed cell performance loss, observed as if the original fuel contains less CO_2 or CH_4.

Process integration

In this section, a continuous running of the gas producer is first conducted to produce hydrogen-rich gas from a simulated biogas (40 vol. % CO_2), by putting together all the individual reactions examined earlier. This is then succeeded with running the model PEFC stack on the acquired hydrogenous gas to demonstrate the suitability of the gas for PEFC.

Production of hydrogen-rich gas As a summary of the preceding examinations for individual reactions, Table 2 shows the suitable operating conditions for all the reactions involved in the hydrogen-rich gas producer illustrated in Figure 2. In the table, the stated temperatures referred to the ones that might be usually adopted in operation, whereas the space velocities mentioned their highest permissible values. For PROX, the temperature 403 K denotes actually the middle-point value of its suitable temperature range from 373 to 423 K. Presumably setting the temperature at this value may prevent the actual working T_{PROX} from being out of its suitable temperature range (373 to 423 K), even when the heat management is poor (such as with over or insufficient cooling). Furthermore, for PROX, the table preferred a slightly higher O/CO ratio (3.0) than the tested value in Figure 9 (near 2.5). This is for a thorough oxidation of CO in PROXr, because one would never adventure to damage the downstream PEFC by an insufficient CO removal. In reference to steam ratios, it is noteworthy that to ensure the ratio of steam/gas=1.2 for HTS, additional steam has to be added to HTSr, when RFM has a steam/CH_4 ratio around 2.7/1.5. Then, moving part or all of the steam feed for HTSr to RFMr, may provide the gas producer an optimized operation, because this allows a higher Steam/CH_4 ratio in RFMr to facilitate the reforming reactions, although dose not vary much the steam/gas ratio for HTS.

Summarized in Table 3 are the precise conditions, decided according to Table 2, for the continuous test on the hydrogen-rich gas producer. The O/CO ratio presented was not a single value, but a range, because it was estimated from the measured CO concentration at the LTSr exit, and the concentration more or less fluctuated during the running. Also, due to the fluctuations in the CO concentration, rather higher O/CO ratios, compared to Table 2, were employed to absorb the possibly instant peaks of CO released from the LTSr (Van Keulen and Reinkingh, 1999).

Figure 13 shows the outlet concentrations of gas components (a) H_2, (b) CO_2, (c) CO, and (d) CH_4, from all the four reactors. As it should be, the hydrogen concentration became gradually higher from RFMr to LTSr. Through the last reactor PROXr it became slightly lower due to the H_2 consumptions in the oxidation via excessive O_2, and in the methanation of CO and

Table 2. Necessary Conditions for the Reactions Involved in the Hydrogen-Rich Gas Producer in Figure 2 and over the Industrial Catalysts Specified in Table 1

Reaction	Temp. [K]	$Sv_{st,dry}$ [ml/(g · h)]	Steam [v/v]	O/CO [v/v]	Criterion or Objective
RFM	~1063(1)	<12000	Steam/CH_4 ≥ 2.7:1.5	—(2)	Converted CH_4 > 98%
HTS	~703	<3500	Steam/Gas ≥ 1.2:1.0	—	Outlet CO < 10.0 vol.%
LTS	~503	<3200	Left steam after LTS	—	Outlet CO < 1.0 vol.%
PROX	~403	<8000	—	~3.0	Outlet CO < 10 ppm

(1) "~" means around the value indicated.
(2) "—" means no definition.

Table 3. Reaction Conditions for the Long-Time Continuous Test Shown in Figure 13

Reactor	Conditions (Raw Gas: CH_4:CO_2 = 1.5:1.0 v/v)			
RFMr(1)	Cat. = 4.5 g,	T_{RFM} = 1063 K,	$Sv_{st,dry}$ = 6210 ml/(g · h),	Steam/CH_4 = 3.12 v/v
HTSr	Cat. = 45.0 g,	T_{HTS} = 703 K,	$Sv_{st,dry}$ = 1780 ml/(g · h),	Steam/Gas = 1.27 v/v
LTSr	Cat. = 45.0 g,	T_{LTS} = 503 K,	$Sv_{st,dry}$ = 1890 ml/(g · h),	Steam/Gas = 1.08 v/v
PROXr(2)	Cat. = 20.0 g,	T_{PROX} = 403 K,	$Sv_{st,dry}$ = 4700 ml/(g · h),	O/CO = 3.1 ~ 3.4 v/v

(1) Corresponding to the slightly higher steam feed to RFMr (Steam/CH_4 = 4.7/1.5), less steam was fed to HTSr so that the Steam/Gas ratio for HTS remained to be close to 1.2.
(2) Slightly excessive oxygen (O/CO > 3.0) was fed to PROXr to absorb the fluctuations in CO concentration at the exit of LTSr.

CO_2. Figure 13a also showed the H_2/CO ratio in the reformate from RFMr, showing a value higher than 3.0. This resulted just from the higher steam/CH_4 ratio (about 3.1) for RFM realized by moving part of the steam feed supposed for HTSr to RFMr. Corresponding to the gradually deeper WGS from RFMr to LTSr, the CO_2 fraction successively increased (Figure 13b), whereas the CO concentration gradually decreased (Figure 13c). In Figure 13c, the CO concentration (about 20 vol. %) after RFMr was lowered to 7.0 vol. % through HTS, and this was further decreased to about 0.5 vol. % via LTS. From a thermodynamic aspect we may say that such a CO-partition among the three reactors is reasonable. After PROX, the CO content had become undetectable. Since our measuring system allowed a few of ppm CO to be measured, the result indicates in fact a complete removal of the CO from LTSr in PROXr. The CH_4 fraction was gradually lower until PROXr (Figure 13d), showing essentially that in HTSr and LTSr there was not obvious CH_4 formation, and the increased dry-gas volume via WGS was responsible for the gradually smaller CH_4 fraction. After PROX, some CH_4 was formed from methanation, although on the other hand there was a slight decrease in dry-gas volume due to the consumption of H_2 as well as of CO and CO_2. An evident rise in the CH_4 fraction exhibited, thus, from LTSr to PROXr. Nonetheless, the CH_4 content in the final hydrogen-rich gas (from PROXr) is residual, such as less than 0.15 vol. % in Figure 13d. For the test in Figure 13, the CH_4 conversion in RFMr was about 99.5%.

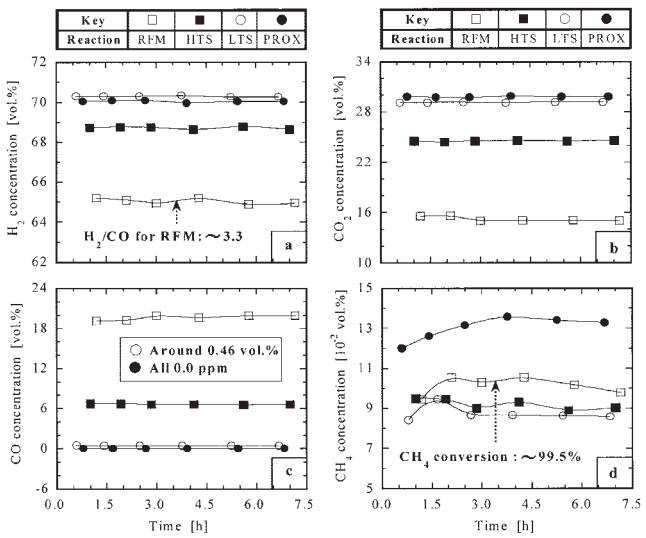

Figure 13. Gas compositions at the exits of the involved reactions in a long-time continuous test of the whole producer (test conditions being detailed in Table 3).

The test in Figure 13 lasted for more than 7 h, but there was no obvious variation for all the measured gas concentrations. This shows the stability of the catalysts as well as of the whole system. More confidently, this stability was shown also in our tests with regard to individual reactions detailed in the previous section. Instead of replacing catalyst day by day, we usually used each of the loaded catalyst for many days, that is, for several tens of hours, with many times cooling and heating. Even so, no significant deactivation had been observed, as long as enough steam was fed for the catalysts of RFM, HTS and LTS.

In addition, Figure 13 shows that the acquired hydrogen-rich gas contained H_2 about 70 vol. %, CO_2 around 30 vol. %, and CH_4 residually. Changing the CH_4 content in the feed between 50 and 70 vol. % may vary the H_2 and CO_2 fractions, but the variation would be no more than 5 vol. %. The gas from LTSr had almost the same composition as the final hydrogenous gas from PROXr did, but the former contained more CO of up to 1.0 vol. %. For RFM, the steam/CH_4 ratio played an important role on the composition of the reacted gas. The lower the steam ratio, the higher its CO fraction, while the lower its H_2 and CO_2 concentrations would be (Effendi et al. 2002). At the steam ratios higher than 1.8, the outlet CO fraction was usually less than 28 vol. %, although the corresponding H_2 concentration was around 64 vol. %.

Application to PEFC stack. Hydrogen-rich gases produced from three differently composed model biogases were applied to the 50-watt model PEFC stack to demonstrate the adaptation of the producer, as well as of the PEFC to various different biogas fuels. The gas productions were under the same conditions as for the continuous test depicted above (that is, the same catalyst amounts, temperatures, steam, and oxygen ratios). Plotted in Figure 14 are the acquired voltage-current and power-current curves for the stack. The stated equivalent H_2 rate (by legend) was calculated from the gas flow rate and gas composition measured after PROXr. According to the given "raw feed", that is, the rates of CH_4 and CO_2 ("CH_4+CO_2"), one can figure out that the CH_4 contents of the examined feedstock were 62.3, 51.2, and 59.5 vol. % for the legends ■□, ●○ and ▼▽, respectively. These values included possibly the lowest CH_4 concentrations for realistic biogas. As generally known, the lower the CH_4 content, the more difficult it would be to run the PEFC on biogas-based fuel.

The overall characteristics of the voltage-current and power-current curves are similar as those shown in Figure 10. However, the voltages, in turn the powers, were not higher in Figure 14 at the higher H_2 feed rates (1.65 compared to 1.5, and 1.35

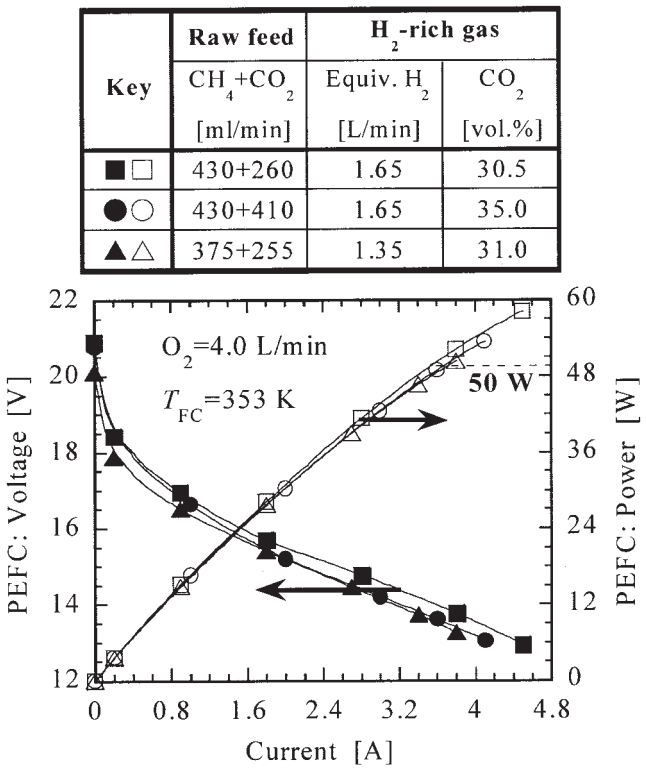

Figure 14. Performance of the 50W model PEFC stack run on the hydrogen-rich gas produced from simulated clean biogas.

compared to 1.2 in Figure 10). At higher currents, such as larger than 3.0 A, the voltage and power outputs were even lower than those in Figure 10. It was observed that at such higher currents the cell voltage decreased more rapidly with increasing the current. This implies a lower limit current for the case using hydrogen-rich gas produced from biogas (compared to pure-H_2 fuel). All of these revealed a decreased performance of the stack, just complying with the previously clarified influence of CO_2 through Figure 11. In addition to CO_2 (>30 vol. %), the residual CH_4 in the hydrogenous gas would add a degrading effect to the cell performance as well. Notwithstanding, the result of Figure 14 is encouraging. The model PEFC stack worked normally even when the raw gas (simulated biogas) contained CO_2 up to 49 vol. % (●○). Also, the desired fifty-watt power was steadily achieved for all the tested cases (being afraid of damaging the stack the rather higher currents not being tested). No matter how biogas varies its CH_4 content between 50 and 70 vol. %, such an output would be quite confident at the equivalent H_2 feed rates not much less than 1.6 L/min (see also Figure 11).

Figure 15 demonstrates the stability of the power output from the PEFC stack. The tested gas was the same as indicated in Figure 14 by the legend ■, and the test itself succeeded the measurements for Figure 14 under maintained operating conditions for both the hydrogen-rich gas producer and the PEFC stack. Thus, the actual time of continuously running the model stack was about 7 h. The equivalent H_2 flow rate and CO_2 fraction mentioned in Figure 15 refer to their average values during the time for stability testing (about 2.5 h). From the figure we can see that the voltage and power outputs had some slight fluctuations, but on the whole they were stable. There had thus an average output of 13.5 V in voltage, and 54.0 W in power for the examined conditions. The whole system (Figure 1) from gas production to PEFC stack included many reactors, controllers (for flows, temperatures, and so on), connection pipes, and valves. Having some slight fluctuations in the final power output is, therefore, imaginable. The fluctuations might come from variations in, such as hydrogen-rich gas amount and composition, and PEFC working temperature.

An approximate calculation of the hydrogen utilization for electricity generation can be made on the basis of Figures 14 and 15. Analyzing Figure 10 had shown that the hydrogen consumed for the specified 50-watt power in the model PEFC stack was about 0.7 L/min. Thus, at the hydrogen feed rate of 1.6 L/min only 44% of the supplied H_2 was estimated to consume for electricity generation, which is much lower than the generally expected hydrogen-utilization efficiency of about 80%. Although, the energy in the unconverted H_2 can be recovered after the PEFC stack through, for example, generating heat, the hydrogen-utilization efficiency for the stack still needs to be improved. For our case, the major factor that restricted the H_2 utilization for electricity was the low-limit currents of the tested cells. If the cells were improved, for example, by using PtRu instead of Ru as their anode catalyst, to be more tolerant to CO_2 as well as to CH_4, such that the cell stack could work at higher currents, such as at 6.0 A, there must be much increased percentages of H_2 being used for electricity. This indicates then an important future work for the proposed PEFC system using biogas as fuel. That is to develop fuel cells that enable high-working currents with fuels containing CO_2 of up to 35 vol. % and CH_4 of up to 4.0 vol. %.

Concluding Remarks

This article provided the basic technical data for hydrogen-rich gas production from desulfurized anaerobic digestion bio-

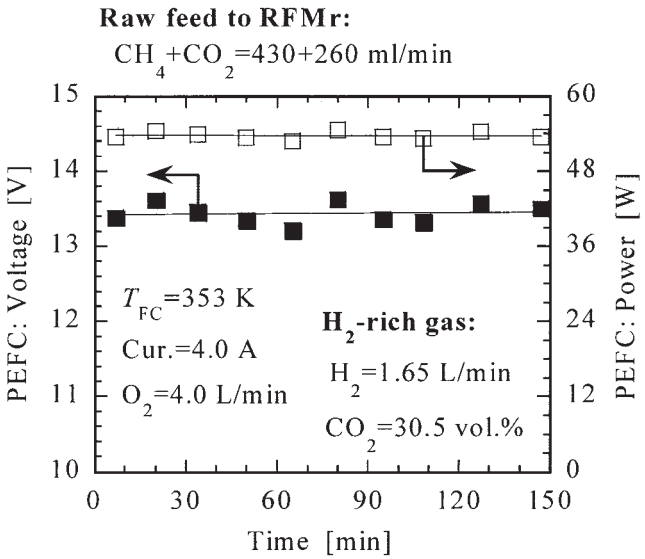

Figure 15. Output stability of the model PEFC stack run on the hydrogen-rich gas produced from simulated clean biogas.

gas, and demonstrated the possible application of the produced hydrogenous gas to the polymer electrolyte fuel cell (PEFC). The relevant experiments for gas conversion were carried out over industrial catalysts, using a stainless-steel-made hydrogen-rich gas producer specifically designed for providing fuels for a 50-watt model PEFC stack. The results showed that it is definitely possible to convert the anaerobic digestion biogas (composition: 50–70 vol. % CH_4, 30–50 vol. % CO_2) into PEFC-usable hydrogen-rich gas through a gas producer, consisting of a steam reformer (RFMr), two water-gas-shift (WGS) reactors at high (HTSr) and low (LTSr) reaction temperatures, respectively, and a selective CO oxidizer (PROXr). The acquired hydrogen-rich gas contained usually 70 vol. % H_2, 30 vol. % CO_2, and residual CH_4 ($<$1.0 vol. %). All CO generated in methane reforming can be reduced to less than 1.0 vol. % via HTS and LTS in succession, although the left CO after LTS is definitely removable to less than 10 ppm via PROX. The resultant hydrogenous gas from PROXr is directly applicable to the PEFC. Stable power generations were identified with the model PEFC stack, but the alien gas species CO_2 as well as CH_4 present in the gas considerably reduced the cell performance. Compared to pure hydrogen, the hydrogen-rich gas acquired from (simulated) biogas exhibited not only a lower-voltage and power output for each given current, but also a smaller limit current (maximal allowable current). The latter significantly lowered the maximal available power from the cell stack, and the hydrogen utilization efficiency for electricity. This was suggested to be one of the important technical problems requiring to be overcome for further development of the PEFC system using biogas as fuel.

With the industrial catalysts tested in this article, the individual reactors for the hydrogen-rich gas producer (that is, from RFMr to PROXr) should be necessarily operated under the conditions specified in Table 2. Those conditions are also generally applicable to other methane reforming systems using the same catalysts. Furthermore, the article demonstrated that the WGS surely coexists with CH_4 reforming in RFMr, and the CO methanation during PROX can extend the temperature window of CO oxidation. On the basis of these some further optimizations for the hydrogen-rich gas producer were highlighted. The article clarified also that the PEFC performance loss with the presence of CO_2 in hydrogen fuel gas was more serious at higher CO_2 fraction, especially when the fraction was over 20 vol. %. At such high CO_2 fractions, the CO_2-induced performance loss was much larger than that caused by the residual CH_4 of up to 4.0 vol. %.

Acknowledgments

The authors are grateful to Mr. M. Yamamoto of AIST Hokkaido for his help on the experiments, and to Ms. N. Imai of the same Institute for her measurements of catalyst properties. Thanks also extended to Mr. Y. Mitarai of Biotech, Ltd., Japan, and to Mr. J. Watanabe of Suzuki Shoko, Ltd., Japan, for their documentary work in organizing the research. The research was partially financed by The Ministry of Agriculture, Forestry and Fisheries, Japan. The manuscript for the article was prepared during the first author's visit to Germany as an Alexander von Humboldt-Stiftung research fellow.

Literature Cited

Ascoli, A., J. D. Pandya, and G. Redaelli, "Electrical Chracterization of a 2.5 kW Phosphoric Acid Fuel Cell Stack Operating on Simulated Reformed Biogas," *Energy*, **14**, 875 (1989).

Ball, S., A. Hodgkinson, G. Hoogers, S. Maniguet, D. Thompsett, and B. Wong, "The Proton Exchange Membrane Fuel Cell Performance of a Carbon Supported PtMo Catalyst Operating on Reformate," *Electrochem. Solid-State Lett*., **5**, A31 (2002).

Bischoff, M., and G. Huppmann, "Operating Experience with a 250 kW (el) Molten Carbonate Fuel Cell (MCFC) Power Plant," *J. Power Sources*, **105**, 216 (2002).

Chawla, S. K., and K. K. Ghosh, "Thermodynamic Analysis of Hydrogen Production from Biogas for Phosphoric Acid Fuel Cell," *Int. J. Hydrogen Energy,* **17**, 405 (1992).

Choudhary, V. R., B. S. Uphade, and A. S. Mamman, "Simultaneous Steam and CO_2 Reforming of Methane to Syngas over NiO/MgO/SA-5205 in Presence and Absence of Oxygen," *Appl. Catal. A: Gen*., **168**, 33 (1998).

De Bruijn, F. A., D. C. Papageorgopoulos, E. F. Sitters, and G. J. M. Janssen, "The Influence of Carbon Dioxide on PEM Fuel Cell Anodes," *J. Power Sources*, **110**, 117 (2002).

Dhar, H. P., L. G. Christner, A. K. Kush, and H. C. Maru, "Performance Study of a Fuel Cell Pt-on-C Anode in Presence of CO and CO_2, and Calculation of Adsorption Parameters for CO," *J. Electrochem. Soc*., **133**, 1574 (1986).

Effendi, A, Z.-G. Zhang, K. Hellgardt, K. Honda, and T. Yoshida, "Steam Reforming of a Clean Model Biogas over Ni/Al_2O_3 in Fluidized- and Fixed-Bed Reactors," *Catal. Today*, **77**, 181 (2002).

Hammad, M., D. Badarneh, and K. Tahboub, "Evaluation Variable Organic Waste to Produce Methane," *Waste Energy Convers. Manage.*, **40**, 1463 (1999).

Huang, J., and R. J. Crookes, "Assessment of Simulated Biogas as a Fuel for the Spark Ignition Engine," *Fuel*, **77**, 1793 (1998).

Karim, G. A., and I. Wierzba, "Methane-Carbon Dioxide Mixtures as a Fuel," *SAE Special Publications*, No. 927, Paper 921557, p. 81-91 (1992).

Naumann, S. T., and C. Myrén, "Fuel Processing of Biogas for Small Fuel-cell Power-Plants," *J. Power Sources*, **56**, 45 (1995).

Neyeloff, S., and W. Gunkel, "Performance of a CFR Engine Burning Simulated Anaerobic Digester's Gas," *ASAE*, **81**(4), 324 (1981).

Oh, S. H., and R. M. Sinkevitch, "Carbon Monoxide Removal from Hydrogen-Rich Fuel Cell Feedstreams by Selective Catalytic Oxidation," *J. Catal*., **142**, 254 (1993).

Pandya, J. D., K. K. Ghosh, and S. K. Rastogi, "A Phosphoric Acid Fuel Cell Coupled with Biogas," *Energy*, **13**(4), 383 (1988).

Staniforth, J., and K. Kendall, "Biogas Powering a Small Tubular Solid Oxide Fuel Cell," *J. Power Sources*, **71**, 275 (1998).

Staniforth, J., and K. Kendall, "Cannock Landfill Gas Powering a Small Tubular Solid Oxide Fuel Cell-A Case Study," *J. Power Sources*, **86**, 401 (2000).

Staniforth, J., and M. Ormerod, "Implications for Using Biogas as a Fuel Source for Solid Oxide Fuel Cell: Internal Dry Reforming in a Small Tubular Solid Oxide Fuel Cell," *Catal. Lett*., **81**, 19 (2002).

Shiga, H., K. Shinda, K. Hagiwara, A. Tsutsumi, M. Sukurai, K. Yoshida, and E. Bilgen, "Large-Scale Hydrogen Production from Biogas," *Int. J. Hydrogen Energy*, **23**, 631 (1998).

Sishtla, C., G. Koncar, R. Platon, S. Gamburzev, A. J. Appleby, and O. A. Velev, "Performance and Endurance of a PEMFC Operated with Synthetic Reformate Fuel Feed," *J. Power Sources*, **71**, 249 (1998).

Snytnikov, P. V., V. A. Sobyanin, V. D. Belyaev, P. G. Tsyrulnikov, N. B. Shitova, and D. A. Shlyapin, "Selective Oxidation of Carbon Monoxide in Excess Hydrogen over Pt-, Ru- and Pd-Supported Catalysts," *Appl. Catal*., **239**, 149 (2003).

Tabata, T., "Technology for Fuel Reforming," *Development and Application of Polymer Electrolyte Fuel Cell*, NTS (Ltd.), ed., NTS Publication, Tokyo, pp. 233-237 (2000).

Van Keulen, A. N. J., and J. G. Reinkingh, "Hydrogen Purification," U. S. Patent, No. 6403049 (2002).

VanderWiel, D. P., M. Pruski, and T. S. King, "A Kinetic Study on the Adsorption and Reaction of Hydrogen Over Silica-Supported Ruthenium and Silver-Ruthenium Catalysts During the Hydrogenation of Carbon Monoxide," *J. Catal*., **188**, 186 (1999).

Weiland, P., "Anaerobic Waste Digestion in Germany-Status and Recent Development," *Biodegradation*, **11**, 415 (2000).

Wilson, M. S., C. Derouin, J. Valerio, and S. Gottesfeld, "Electrocatalysis Issues in Polymer Electrolyte Fuel Cells," *Proc. Twenty Eighth Intersociety Energy Convers. Eng. Conf*., Atlanta, Vol. 1, published by ACS, Washington, DC, 1203 (1993).

Zhang, Z. G., A. Effendi, X. Chen, K. Honda, and T. Yoshida, "Hydrogen

Production from Biogas through Steam Reforming Followed by Water Gas Shift Reaction and Purification with Selective Oxidation Reaction," *Proc. First Int. Conf. on Greenhouse Gases and Animal Agriculture*, J. Takahashi and B. A. Young, eds., Elsevier , Amsterdam, p. 275-279 (2002).

Zhang, Z. G., G. Xu, X. Chen, K. Honda, and T. Yoshida, "Process Development of Hydrogenous Gas Production for PEFC from Biogas," *Fuel Proc. Technol.,* **85**, 1213 (2004).

Appendix

For CH_4-based feedstock, the following are the possible reactions involved in RFMr, HTSr and LTSr

$$\text{Steam reforming} \quad CH_4 + H_2O \leftrightarrow 3H_2 + CO \tag{A1}$$

$$CO_2 \text{ reforming} \quad CH_4 + CO_2 \leftrightarrow 2H_2 + 2CO \tag{A2}$$

$$\text{CO water-gas-shift} \quad CO + H_2O \leftrightarrow H_2 + CO_2 \tag{A3}$$

and

$$\text{Reforming-shift complex} \quad CH_4 + 2H_2O \leftrightarrow 4H_2 + CO_2. \tag{A4}$$

This allows the carbon and oxygen balances of the system to be formulated, respectively by

$$aG + bG + G(1 - a - b - c) = I_1 + I_2 \tag{A5}$$

and

$$aG + 2bG = 2I_2 + I_3 \tag{A6}$$

enabling in turn the equations

$$G = (I_1 + I_2)/(1 - c) \tag{A7}$$

for the molar flow rate of the post-reaction dry-gas, and

$$I_3 = G(a + 2b) - 2I_2 \tag{A8}$$

for the moles of reacted steam (H_2O) in unit time. In the above Eqs A5 to A8, the other parameters are a, b, and c for the molar concentrations of CO, CO_2, and H_2 in dry production gas, and I_1 and I_2 for the molar flow rates of the reactants CH_4 and CO_2, respectively.

Manuscript received June 18, 2003, and revision received Jan. 19, 2004.